Time-Frequency Representation Based Approach for Separation of Target Rigid Body and Micro-Doppler Effects in ISAR Imaging

LJubiša Stanković, Thayananthan Thayaparan, Igor Djurović

Abstract— **Micro-Doppler (m-D) effect is caused by moving parts of the radar target. It can cover rigid parts of a target and degrade the ISAR image. Separation of the patterns caused by stationary parts of the target from those caused by moving (rotating or vibrating) parts is the topic of this paper. Two techniques for separation of the rigid part from the rotating parts have been proposed. The first technique is based on time-frequency (TF) representation with sliding window and order statistics techniques. The first step in this technique is recognition of rigid parts in the range/cross-range plane. In the second step, reviewed TF representation and order statistics setup are employed to obtain signals caused by moving parts. The second technique can be applied in the case of very emphatic m-D effect. In the first step the rotating parts are recognized, based on the inverse Radon transform. After masking these patterns, a radar image with the rigid body reflection can be obtained. The proposed methods are illustrated by examples.**

I. Introduction

Micro-Doppler (m-D) effect appears in the ISAR radar imaging when the target has one or more rotating or vibrating parts. This effect can decrease readability of radar images. However, the m-D effect, at the same time, carries information about the features of moving parts (type, velocity, size, ...). Several papers have been written about the ways how to deal with the m-D effect. Wavelet analysis of the helicopter and human data, along with time-frequency (TF) representation based imaging system, is presented in [1], [2], [3]. Details on the m-D effect physics, with some typical examples, are given in [4], [5]. A method for separation of the m-D effect from the radar image, based on the chirplet transform, is proposed in [6]. Part of the radar signal, obtained as a result of the m-D effect, after appropriate separation from the rest of the target radar image, can be used for estimation of rotating part parameters. In [6], the received signal has been expanded into a set of chirplet functions. The obtained chirplet functions are divided into two groups: the chirplets with small chirp-rate parameter (associated to the rigid part) and the chirplets with large chirp-rate parameter (associated to the moving parts). Calculation burden of this procedure is high, since the chirplet dictionary could be extremely large. Both wavelet-based and chirplet based procedures are used in [7] to extract the m-D features such as the rotating frequency of the antenna from SAR data. Analysis of TF representations application in radar target identification is presented in [8]. The reduced interference distributions from the Cohen class are applied as a tool for target identification. A technique for m-D effect estimation from reflected signal, based on the TF signatures and decomposition of basis functions, is presented in [9]. This technique can be used for m-D effect signals that can be represented as sinusoidal FM signals.

Here, two procedures for separation of signals coming from the rigid (slowly moving) body and rotating parts are proposed. In order to analyze the m-D effect, we will perform TF (more accurately space/spatial-frequency) analysis with a sliding window. Based on the order statistics of the obtained TF representations, we will make decision if the compo-

IEEE Trans. on Aerospace and Electronics Systems, Vol. 42, No. 7, Oct. 2006.

nents belong to the rigid body or to the rotating target parts. The other approach is based on the Radon transform (RT). The TF representation of the sinusoidal FM signal can be concentrated in a single point by applying the inverse RT to the TF representation. In this way, patterns of the rotating parts can be easily extracted from the signal mixture.

The paper is organized as follows. The ISAR signals modeling is described in Section II with model of signals caused by rigid body and moving parts of target. Method for separation of the rigid body and moving elements from the radar image, based on the order statistics of the TF representation with sliding window, is given in Section III. Separation of rotating patterns from the radar image by using the inverse RT is presented in Section IV. Simulation study is given in Section V. Concluding remarks with possible directions for further research are given in Section VI.

II. Radar Signal Model

We assume that the signal transmitted toward a radar target consists of M continuos wave signals. Duration of these signals, T_r, is called repetition time. Signal is reflected from target and delayed, attenuated and shifted in frequency. This signal is usually modeled as a sum of point-scatterer responses [4], [6]. Common ISAR imaging model assumes that all point-scatterers share the same angular motion. However, radar target can have moving parts (rotating or vibrating). In this model, the received signal, within the m-th radar sweep, can be written as [6] eq. 1:

$$q_m(t) = \sum_{i=1}^{K} \sigma_i e^{\left(-j\frac{4\pi f}{c}[R_B(t)+x_i\cos\theta_B(t)+y_i\sin\theta_B(t)]\right)} + \sigma_R e^{\left(-j\frac{4\pi f}{c}[R_R(t)+x_R\cos\theta_R(t)+y_R\sin\theta_R(t)]\right)}, \tag{1}$$

where σ_i is the reflection coefficient of the i-th scatterer, f is the radar operating frequency, (x_i, y_i) are coordinates of the scatterer point (x coordinate is in the direction of line-of-sight, according to Fig. 1). Target translation and angular motion are denoted by $R(t)$ and $\theta(t)$, with indices B and R corresponding to the rigid body and rotating parts, respectively. Here we assume a single rotating point. In general, we have radar target with arbitrary number of moving parts. Motion compensation techniques [6], [10] are employed to remove the influence of translation motion. Thus, we can assume that $R_B(t) \to 0$ and $R_R(t) \to 0$. For the main body holds $|\theta_B(t)| \ll 1$. It results in $\cos\theta_B(t) \approx 1$ and $\sin\theta_B(t) \approx \theta_B(t) = \omega_B t$, where ω_B is effective body rotation rate, after motion compensation. This approximation cannot be applied to rotating parts since, $\theta_R(t)$ can vary rapidly. The received signal can now be written as:

$$q_m(t) = \sum_{i=1}^{K} \sigma_i e^{\left(-j\frac{4\pi f}{c}[x_i+y_i\omega_B t]\right)} + \sigma_R e^{\left(-j\frac{4\pi f}{c}[x_R\cos\theta_R(t)+y_R\sin\theta_R(t)]\right)}. \tag{2}$$

The first term in (2) represents sinusoids concentrated at frequencies proportional to y_i, $i \in [1, K]$. Information on other coordinate can be obtained based on processing of all returned radar signals. The radar image is commonly obtained by a 2D FT of the compressed received signal denoted as $q(m,t) \equiv q_m(t)$. The second term in (2) represents sinusoidally modulated FM signal caused by rotating part with a relatively large $\theta_R(t)$ during the repetition interval. This signal can cover large portion of the TF plane. It can mask significant part of the radar image. Influence of rotating and vibrating parts on radar image is commonly referred to as the m-D effect. Detailed considerations of physics of this effect, mathematical derivations and simulation study are given in [4]. This effect should be removed from the radar image of rigid body part, but at the same time it contains important information related to the radar target. In the next section, a technique for separation of the rigid body and rotating parts influence from the received signal is presented. It is based on the running window TF representation and the L-

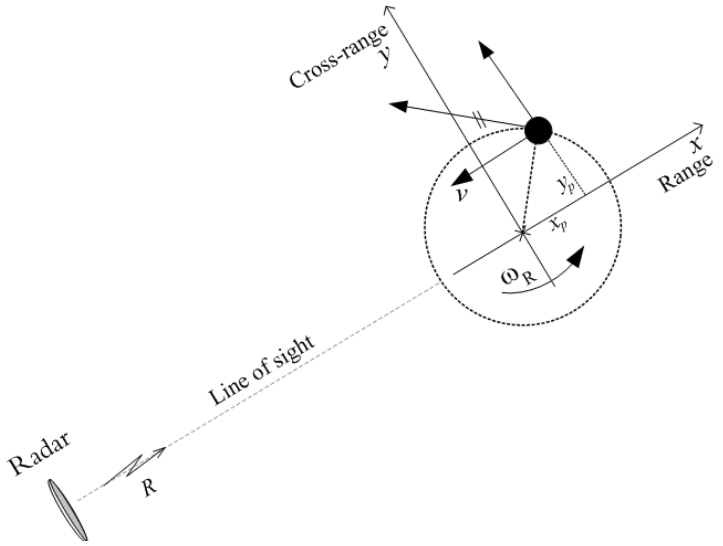

Fig. 1. Illustration of the radar target geometry.

statistics. In Section IV the RT is applied for removing influence of strong rotating parts.

III. Time-frequency analysis and order statistics approach

Basic idea

In order to explain the approach for separation of the m-D effect from the ISAR image, we will consider the experimental setup used in [6]. Target with five scatterers at positions: $(0,0)$, $(\pm 6,0)$ and $(0,\pm 6)$ is considered (positions are in meters). Reflection coefficient for the central point is 5, for the second pair of points it is 1, while for the third pair it is 2. In addition, there is a point rotating at a distance of 0.2m from the center, with reflection coefficient of 3.33. A 10GHz radar with bandwidth of 800MHz is assumed. During coherent integration time the radar body rotated for 4 degrees ($4\pi/180$ Hz). Rotating part has constant angular velocity of 6.67Hz. For analysis of the received signals $q(t,m)$ we will use spectrogram (SPEC) as a TF tool:

$$SPEC(t,\omega_t;m) = \\ = \left| \int_{-\infty}^{\infty} q(t+\tau,m) w(\tau) e^{-j\omega_t \tau} d\tau \right|^2, \quad (3)$$

where $w(\tau)$ is a window function. We will assume that the signal $q(t,m)$ is discretized, producing discretized $SPEC(n,\omega_t;m)$.

The SPEC for various window lengths exhibits different properties for various kinds of signals. The SPEC of the considered radar signal, for a narrow Hanning window with 32 samples, is shown in Fig.2a. The SPEC calculated with a wide Hanning window with 128 samples is depicted in Fig.2b. In both figures we can see stationary patterns, caused by the rigid body, parallel to the time-axis. The SPEC of the rigid body parts is better concentrated for wider than for narrower windows. Also, a sinusoidal pattern caused by the rotating point can easily be seen. It is in accordance with the assumed model for these parts. However, the sinusoidal FM signal is better concentrated for narrower window case.

This example clearly shows that the rigid body and rotating parts in the TF plane should be studied with the TF representation with various window lengths. Upper arrow in Fig.2a denotes frequency where only influence of the rotating parts exists. For that frequency relatively small number of TF samples assume high values. However, in the region of the signal caused by the rigid body (see lower arrow) all TF samples have high values.

For a narrow window in the SPEC we can see that the number of points belonging to the rotating parts is not high as compared to the considered interval. Therefore, we can consider the mean value of the smallest SPEC samples, as a good measure of the rigid body and rotating parts influence. In the region of the rigid body this measure will be high, since the rigid body has influence over the entire considered interval while the influence of the signal caused by rotating part will be removed.

L-statistics

For this kind of analysis a linear combination of order statistics (L-statistics) gives a powerful notational and analytic tool. The L-statistics of the SPEC samples can be defined as [11]:

$$L(\omega_t) = \sum_{n=0}^{N-1} a_n S_{(n)}(\omega_t; m) \tag{4}$$

where $S_{(n)}(\omega_t; m)$ are samples from the set $\mathbf{S}_{\boldsymbol{\omega_t},\mathbf{m}} = \{\mathbf{SPEC}(\mathbf{t}, \boldsymbol{\omega_t}; \mathbf{m}), \mathbf{t} \in [\mathbf{0}, \mathbf{T_r})\}$, sorted into a non-decreasing sequence: $S_{(n)}(\omega_t; m) \leq S_{(n+1)}(\omega_t; m)$. In order to visualize how this measure can be used to distinguish signals caused by various parts of the radar target, we repeat Fig.3a. Three order statistics of this SPEC are presented on the right hand side of this figure (Fig.3b, c and d). They are calculated as:

- $a_n = 4/N$ for $n \in [0, N/4)$ and $a_n = 0$ elsewhere, i.e., for the smallest magnitude SPEC samples (statistics $L_1(\omega_t)$);
- $a_{N/2-1} = a_{N/2} = 1/2$ and $a_n = 0$ elsewhere, i.e., medians of the SPEC values for fixed ω_t (statistics $L_2(\omega_t)$); and
- $a_n = 4/N$ for $n \in [3N/4, N)$ and $a_n = 0$ elsewhere, i.e., for the highest magnitude SPEC samples (statistics $L_3(\omega_t)$).

It can be seen that for the median ($L_2(\omega_t)$), Fig.3c, frequency region of stationary components is noticeable. However, from this illustration it is difficult to recognize that there are three components along y-direction. From Fig.3b, again, the region of stationary components can be seen. In addition, from three peeks we can make the conclusion that scatterers are located at three different y-positions. In addition to the complex sinusoidal components in the third case, Fig.3d, the sinusoidal FM signal region can be seen. These three simple functions will be used in construction of indicators for the region of rigid body and the region of rotating parts. Several modifications will also be made in order to take advantage of two-dimensional structure of the signal $q(t, m)$, as well as to keep calculation burden within a reasonable limit.

Algorithm

Let us introduce the following notation: $I(\omega_t, \omega_m) = I_{\mathrm{RIG}}(\omega_t, \omega_m) \cup I_{\mathrm{MOV}}(\omega_t, \omega_m)$, where $I(\omega_t, \omega_m)$ is a function indicating the region in range/cross-range domain with components caused by target (both from rigid and rotating parts), while $I_{\mathrm{RIG}}(\omega_t, \omega_m)$ is the region of rigid part; and $I_{\mathrm{MOV}}(\omega_t, \omega_m)$ is the region of moving parts. In general, $I_{\mathrm{RIG}}(\omega_t, \omega_m) \cap I_{\mathrm{MOV}}(\omega_t, \omega_m) \neq \emptyset$ holds. Domain (ω_t, ω_m) will be referred hereafter as the range/cross-range domain, since it can be easily transferred to the positions (x, y) of radar target.

As an indicator of target in the range/cross-range domain the following simple criterion will be used:

$$I(\omega_t, \omega_m) = \begin{cases} 1 & |Q(\omega_t, \omega_m)| > \\ & \frac{1}{MN} \sum_{\omega_t} \sum_{\omega_m} |Q(\omega_t, \omega_m)| \\ 0 & \text{elsewhere,} \end{cases} \tag{5}$$

where $Q(\omega_t, \omega_m)$ is a 2D FT of $q(t, m)$. This is a very conservative measure, since the global threshold used here is equal to the mean of $|Q(\omega_t, \omega_m)|$, calculated in the entire range/cross-range domain.

Consider a 2D SPEC of the received signal:

$$SPEC(t, \omega_t; m, \omega_m; N_w, M_w) = \left| \int_{-\infty}^{\infty} \sum_{\Delta m=0}^{M-1} q(t+\tau, m+\Delta m) \times w(\tau, \Delta m) e^{-j\omega_t \tau - j\omega_m \Delta m} d\tau \right|^2. \tag{6}$$

Parameters N_w, M_w are added to denote size of window function $w(\tau, \Delta m)$ in the corresponding directions. Window width M_w is selected as $M_w \approx M$ (number of chirps).

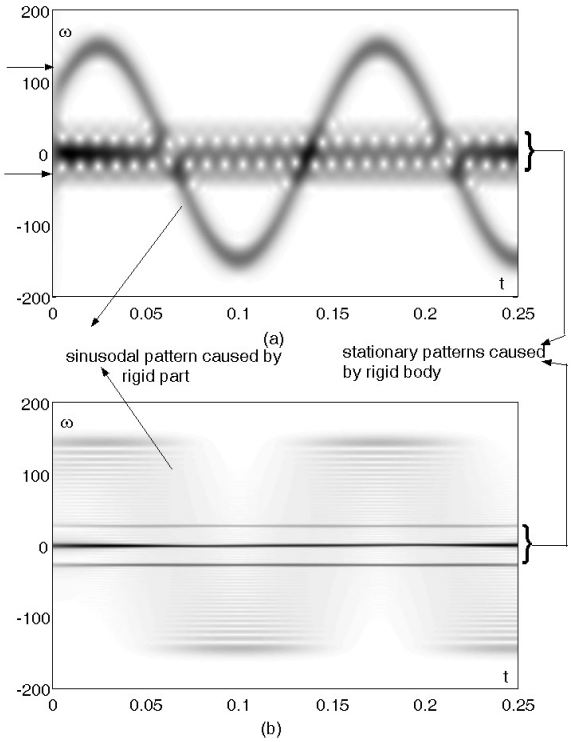

Fig. 2. Spectrogram of radar signal reflected from target with emphatic m-D effect calculated with: (a) Narrow window; (b) Wide window.

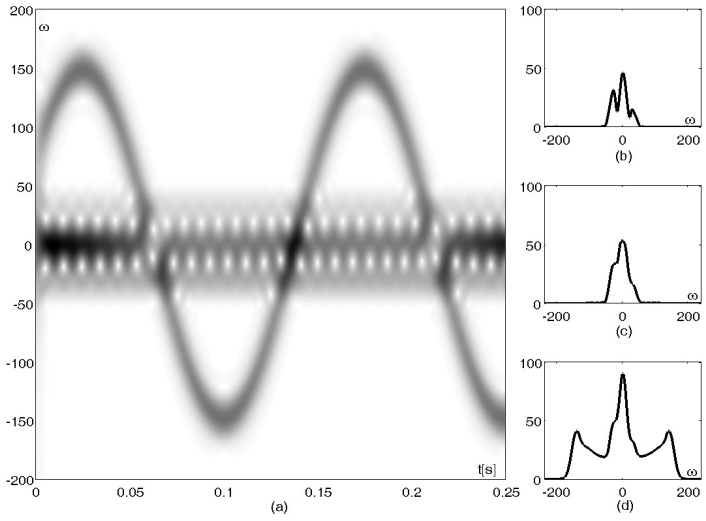

Fig. 3. TF representation and order statistics of the received signal: (a) Spectrogram; (b) $L_1(\omega_t)$; (c) $L_2(\omega_t)$; (d) $L_3(\omega_t)$.

However, narrower windows in t direction are used in order to control concentration of the sinusoidal FM patterns caused by rotating points. Namely, if the window is very wide the TF representation of the sinusoidal FM signal will look like several quasi stationary components [12], see Fig.2b. By decreasing window width we are achieving better concentration of these components around the instantaneous frequency of the sinusoidal FM components. Of course, if we decrease the window length too much the frequency resolution will be decreased and semiperiods of this signal will be connected, resulting again in TF representation degradation.

The above analysis confirms that, in determination of the indicator function, the SPECs should be calculated with various window lengths. We will assume that window lengths are selected from a set $N_w \in \mathbf{N}$, for constant M_w. The SPEC will not be evaluated for each (t, m), but only for equidistantly spaced instants along t direction. Positions are separated for ΔT_{N_w} (for different windows different intervals are used; in our calculation study they are $\Delta T_{N_w} = T_c N/N_w$, $N_w \leq N$). Then, for each point in the range/cross-range domain we calculate:

$$L_{i,N_w}(\omega_t, \omega_m) = \sum_{i=0}^{N-1} a_n S_{(n)}(\omega_t, \omega_m), \qquad (7)$$
$$i = 1, 2, 3$$

where $S_{(n)}(\omega_t, \omega_m)$ are elements from the set:

$$\mathbf{S_{N_w}} = \{\mathbf{SPEC(t, \omega_t; m, \omega_m; N_w, M_w)}, \quad t = t' + l\Delta T_{N_w}, l \in Z\} \qquad (8)$$

sorted into a non-decreasing order $S_{(n)}(\omega_t, \omega_m) \leq S_{(n+1)}(\omega_t, \omega_m)$. Index i denotes earlier introduced form of L-statistics, while N_w denotes length of window function. Based on the above considerations, we get function for the rigid part (sinusoidal components):

$$I_{\mathrm{RIG}}(\omega_t, \omega_m) = I(\omega_t, \omega_m) \prod_{N_w \subset \mathbf{N}} I'_{N_w}(\omega_t, \omega_m), \qquad (9)$$

where $I'_{N_w}(\omega_t, \omega_m)$ can be defined as eq. 10 at the top of the next page.

The first condition in (10) is equivalent to (5), while the second condition is introduced to further emphasize the local maxima, corresponding to the scattering points. It compares values of L_{1,N_w} samples (smallest SPEC samples) in a close neighborhood of the considered point (ω_t, ω_m) with those in a wider neighborhood ($K_1 < K_2$ and $L_1 < L_2$).

For the widest window from the set, the function $|L_{1,N_w}(\omega_t + k_1\Delta\omega_t, \omega_m + l_1\Delta\omega_m)|$ would be well concentrated around the frequency of the rigid body signal components. The sinusoidal FM components, that are spread in the TF plane (see Fig.2a), could have high values of this function. However, for a narrow window, the function $|L_{1,N_w}(\omega_t + k_1\Delta\omega_t, \omega_m + l_1\Delta\omega_m)|$ would be spread around the rigid body components, while the rotation components will be eliminated. Therefore, the product of $I'_{N_w}(\omega_t, \omega_m)$ in (9) will produce function that is equal to 1 for very narrow region in the range/cross-range domain (as in the case of used wide window) with eliminated influence of the rotation parts (as in the case of using narrow window).

The remaining problem is in determining the patterns representing moving objects. The indication of moving object parts is described as:

$$I_{\mathrm{MOV}}(\omega_t, \omega_m) = \\ = I(\omega_t, \omega_m) I''_{N_w}(\omega_t, \omega_m) \Lambda(\omega_t, \omega_m) \qquad (11)$$

where:

$$I''_{N_w}(\omega_t, \omega_m) = \begin{cases} 1 & L_{3,N_w}(\omega_t, \omega_m) \geq \\ & (1+\beta) L_{2,N_w}(\omega_t, \omega_m) \\ 0 & \text{otherwise.} \end{cases} \qquad (12)$$

Indicator function $I''_{N_w}(\omega_t, \omega_m)$ will be equal to 1 for regions in the range/cross-range domain where ratio between the highest and median SPEC samples is higher than $(1 + \beta)$. In our analysis $\beta = 1$ is used. This indicates that, along with stationary pattern, there could exist a pattern caused by moving objects, increasing values of the SPEC at some instants of the TF plane. The remaining problem is to remove possible influence of side lobes caused by stationary pattern from the product $I(\omega_t, \omega_m) I''_{N_w}(\omega_t, \omega_m)$. To this aim we form a

$$I'_{N_w}(\omega_t,\omega_m)=\begin{cases}1 & \begin{array}{c}L_{1,N_w}(\omega_t,\omega_m)\geq\frac{1}{MN}\sum_{\omega_t}\sum_{\omega_m}|L_{1,N_w}(\omega_t,\omega_m)|\ \text{AND}\\ \frac{\sum_{k=-K_1}^{K_1}\sum_{l=-L_1}^{L_1}|L_{1,N_w}(\omega_t+k\Delta\omega_t,\omega_m+l\Delta\omega_m)|}{\sum_{k=-K_2}^{K_2}\sum_{l=-L_2}^{L_2}|L_{1,N_w}(\omega_t+k\Delta\omega_t,\omega_m+l\Delta\omega_m)|}\geq\frac{(2K_1+1)(2L_1+1)}{(2K_2+1)(2L_2+1)}\end{array}\\ 0 & \text{otherwise.}\end{cases}\tag{10}$$

function $\Lambda(\omega_t,\omega_m)$ as:

$$\Lambda(\omega_t,\omega_m)=1-\text{dilate}(I_{\text{RIG}}(\omega_t,\omega_m))\tag{13}$$

where "dilate" denotes dilatation, a morphological operation that extends argument matrix (under extension we assume that neighboring region around $I_{\text{RIG}}(\omega_t,\omega_m)=1$ becomes also equal to 1) [13]. Function $\text{dilate}(I_{\text{RIG}}(\omega_t,\omega_m))$ for 3x3 closest samples in the range/cross-range domain can be defined as:

$$\text{dilate}(I_{\text{RIG}}(\omega_t,\omega_m))=$$
$$=\bigvee_{k=-1}^{1}\bigvee_{l=-1}^{1}I_{\text{RIG}}(\omega_t+l\Delta\omega_t,\omega_m+k\Delta\omega_m),\tag{14}$$

where $\bigvee_{k=-1}^{1}a(k)=a(-1)\vee a(0)\vee a(1)$. This form is a dilatation with structural element square. We have introduced dilatation since the indicator function $I_{\text{RIG}}(\omega_t,\omega_m)$ is very sharp. It also includes corresponding peaks only in the range/cross-range-domain. Therefore, the function $\Lambda(\omega_t,\omega_m)$ allows that points that are not close to the rigid body part could be identified as rotating parts.

For separation of the rotating object component we can use product $I_{\text{MOV}}(\omega_t,\omega_m)Q(\omega_t,\omega_m)$. Also, as it can be seen, in the case of moving parts detection we did not employ the multi-window approach, but only a single, relatively narrow, window. Namely, in this case, results obtained for extremely narrow and wide windows are not useful in separation process, while for other windows results are very similar.

Note that the algorithm is derived based on the assumption that the rigid body influenced signal can be modeled as a sum of complex sinusoids. For more complicated target motion patterns, the motion compensation techniques for focusing distorted data should be applied in the first stage of the algorithm [14].

IV. The Radon transform based algorithm for separation of sinusoidal FM signals

The second approach that will be presented in this section is based on the RT. It can be used only for rotating parts of the target that produce pure sinusoidal FM signals. This approach can be applied only in the case when influence of rotating parts is emphatic.

The RT of a point with position (x_r,y_r) is

$$R_r(\rho,\theta)=c_r\delta(\rho-A_r\sin(\theta-\varphi_r)),\tag{15}$$

where c_r corresponds to the reflection of the point, $A=\sqrt{x_r^2+y_r^2}$ and $\varphi_r=\tan^{-1}(y_r/x_r)$. Period of the RT in θ is 2π. It means that the inverse RT of a sinusoidal pattern in the (θ,ρ) plane is a point in the (x_r,y_r) domain. Since rotating parts produce sinusoidal patterns in the TF domain, it means that inverse RT of TF representation of received signal with m-D effects will have peaks at the positions corresponding to the rotating parts. Note that for the inverse RT we should know the period of sinusoidal pattern, which is not known in advance. In addition, the radar signal may consists of several rotating parts with different unknown rotation frequencies. To solve this problem we assigned considered time interval (in TF representation) to a set of possible periods in θ. The whole TF representation is considered as periodic in time with T_p corresponding to periods in θ, for example from $\pi/3$ up to 4π with a step of 0.1π. The value of 4π means that exactly two periods of sinusoidal pattern exist in the TF representation.

When the assumed period matches the true one, the peak in inverse RT is detected at a position defined by $A=\sqrt{x_r^2+y_r^2}$ and $\varphi_r=\tan^{-1}(y_r/x_r)$. In this way, all parameters of the rotating part are known, including frequency of rotation that corresponds to the period assigned for the case where the peak

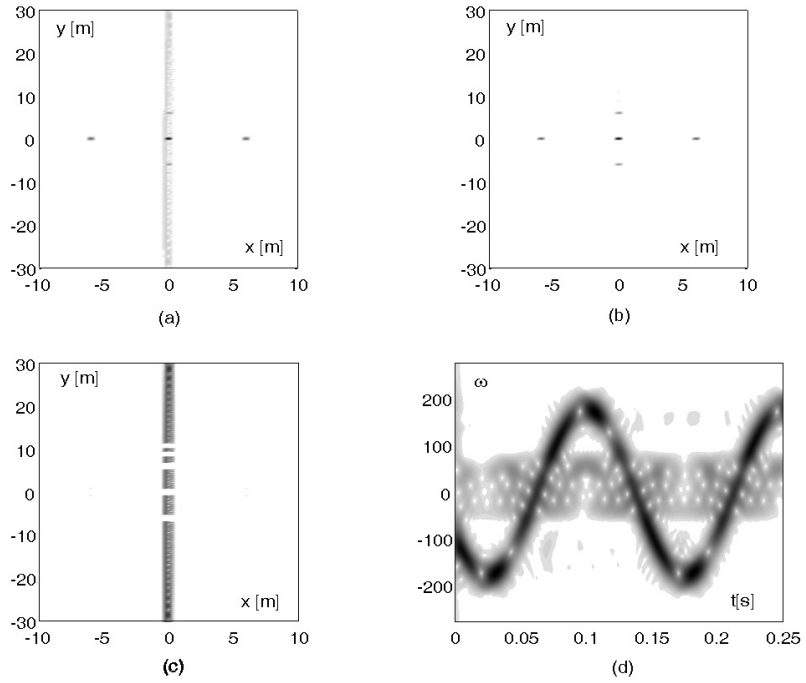

Fig. 4. Separation of rigid body and m-D effect for simple case: (a) $Q(\omega_t, \omega_m)$; (b) Reconstructed radar image; (c) Region of support for sinusoidal FM signal; (d) SPEC of reconstructed m-D signal.

is found. If there are more than one rotating part, with different or the same rotation speed, more peaks will be detected. By filtering the region around the peak and calculating RT of the filtered inverse RT we get clear TF representation of the signal resulting from the rotating parts.

V. SIMULATION STUDY

Example 1: In the first example we considered simulation setup described in Section III and used in [6]. Radar image, including notable m-D effect, is depicted in Fig.4a. The algorithm described in Section III is applied. The Hanning windows are employed along both directions with $M_w = M$ and the set of window lengths in $\mathbf{N} = \{\mathbf{512}, 256, 128, 64, 32, 16, 8\}$ is used. In calculation of $I_{\mathrm{RIG}}(\omega_t, \omega_m)$, expression (9) is applied, where the product $\prod_{N_w \subset \mathbf{N}} I'_{N_w}(\omega_t, \omega_m)$ is calculated iteratively starting from the widest toward narrower windows from the set $\mathbf{N}$. If the resulting product is not changed in consecutive iterations we can stop the procedure. This is an important step, since it significantly reduces calculations in the case of targets without m-D effect. Obtained radar image of the rigid body is depicted in Fig.4b. Parameters $K_1 = L_1 = 1$ and $K_2 = L_2 = 3$ are used in (10). It can be seen that excellent accuracy is achieved. We calculated region of sinusoidal FM component by using (11), with $N_w = 64$. Region of sinusoidal FM signals is given in Fig.4c. In order to demonstrate accuracy of this approach, the reconstruction of sinusoidal FM signal for $m = 0$ is given in Fig.4d. Sinusoidal FM component can easily be recognized from this illustration. At the same time some important features of the moving object can be extracted.

Vibration: This setup has been used for alternative experiment. The same target, but without rotating parts, has been considered. However, the entire target oscillates in the x direction with amplitude of 0.1cm and frequency of oscillations 30Hz. The obtained results are presented in Fig.5. A significant im-

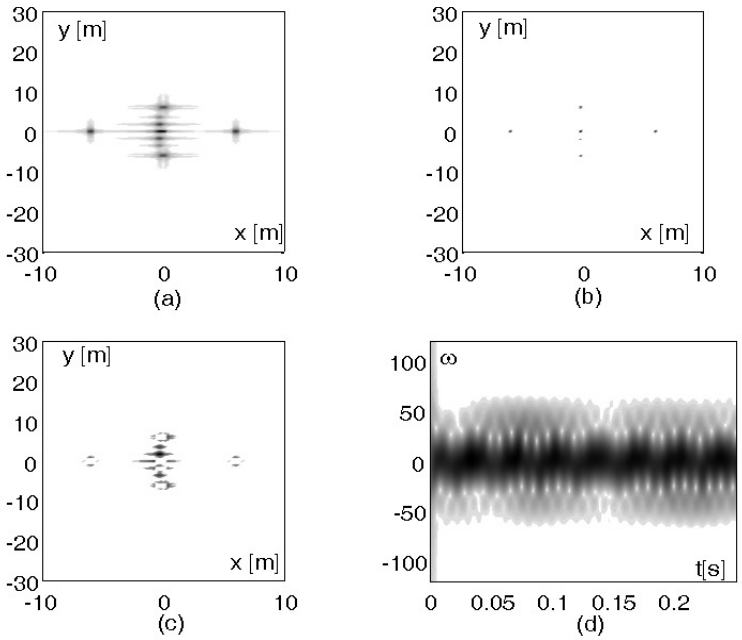

Fig. 5. Separation of rigid body and m-D effect caused with object vibrations: (a) $Q(\omega_t, \omega_m)$; (b) Reconstructed radar image; (c) Region of support for signal caused by vibrations; (d) Spectrogram of reconstructed m-D signal.

provement in radar imagining is achieved with the proposed technique. At the same time, this technique can be used for extraction of the vibration parameters. Note that an analysis of m-D effect for vibrating targets in SAR systems is given in [7], [15].

Example 2: A more complex object, with 45 scatterers: $\{(k,0)$ for $k \in [-6,6]$, $(0,k)$ for $k \in [-6,-1] \cup [1,6]$, $(k, \pm(6-k))$ for $k \in [1,5]$ and $(k, \pm(6+k))$ for $k \in [-5,-1]\}$, is considered. All scatterers have the same reflection coefficient, set to 2. There are two rotating parts. The first is the same like in the previous example, while the second rotates at the distance of 0.5 m from center with radial velocity 2Hz. Reflection of the second rotating part has been set to 7. The same analysis, with the same algorithm setup, like in the previous example is performed. Obtained results are depicted in Fig.6. It can be seen that the reconstruction of objects has been done in a very accurate way. At the same time, reconstruction of the signal caused by rotating parts is good.

Radon transform based algorithm: In this case we also apply the inverse RT, assuming that TF representation pattern is periodic with periods from $\pi/3$ to 3π, with step of $\pi/18$. Two peaks of the inverse RT concentration are detected at two different periods, amplitudes and phases Fig.7. Calculating the RT of the inverse RT filtered around these peaks, we got representation presented in Fig.8, producing very accurate reconstruction of the rotating parts in the TF domain.

UH-1D Helicopter: In this example we consider simulated signal of a German Air Force Bell UH-1D Helicopter known also as 'Iroquois'. Simulation is performed according to [4]. Several effects are emphasized in the TF representation Fig.9a. Stationary patterns along time-axis correspond to the rigid body reflection, vibration of the target or radar-clutter caused by moving in the target background. Motion of two main blades is modeled by two rotating reflectors, producing sinusoidal FM signals with a large magnitude in frequency direction, (1). Main rotor flashes

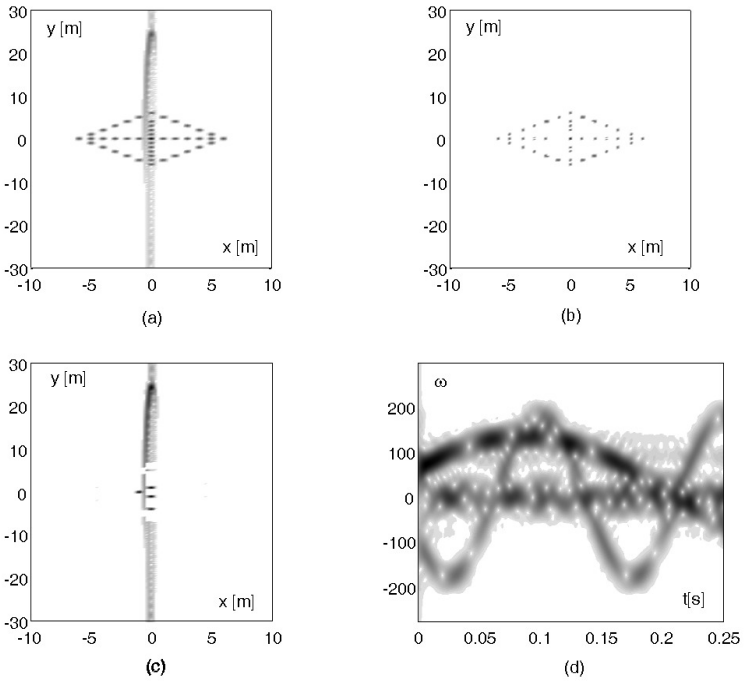

Fig. 6. Separation of rigid body and m-D effect for two moving points: (a) $Q(\omega_t, \omega_m)$; (b) Reconstructed radar image; (c) Region of support for sinusoidal FM signal; (d) SPEC of reconstructed m-D signal.

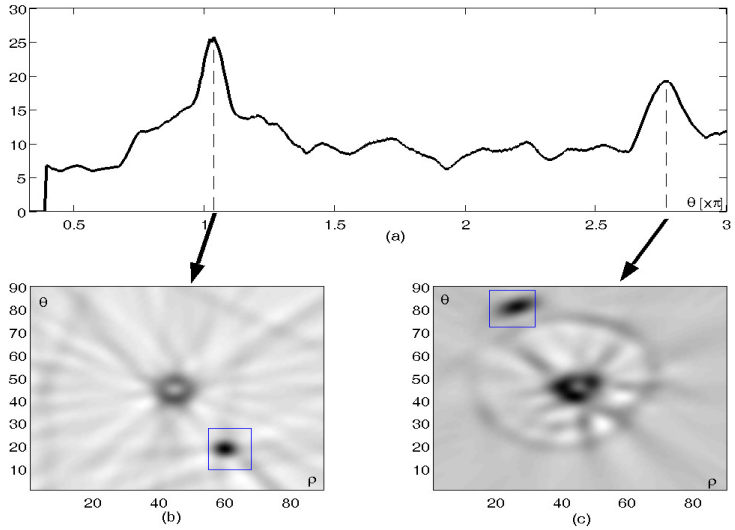

Fig. 7. Concentration measure of the inverse RT of the radar signal TF representation as a function of the assumed angle number (top), with the inverse RT at two positions where maxima are found (bottom).

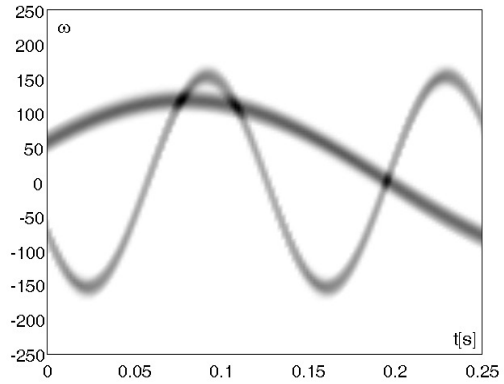

Fig. 8. TF representation corresponding to rotating parts in the last example, obtained by using filtered inverse RT.

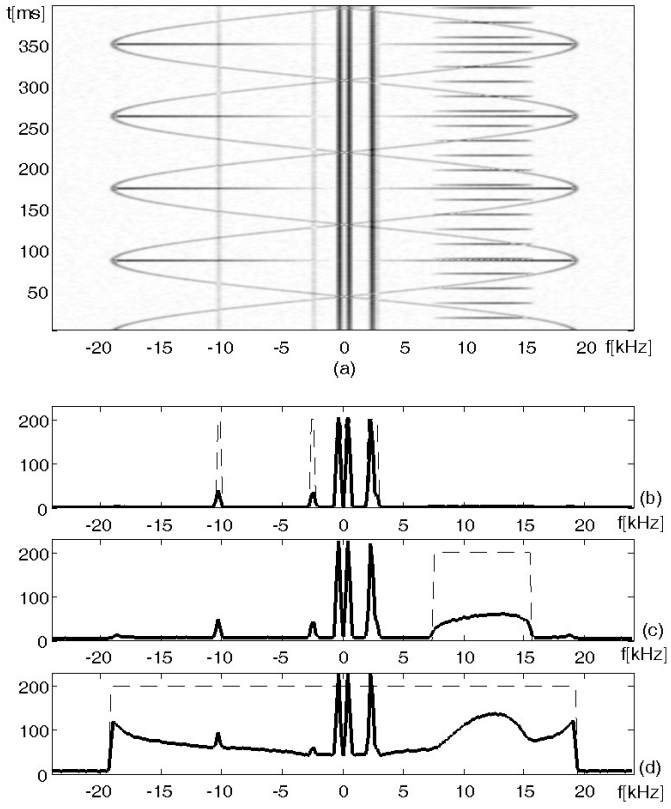

Fig. 9. Radar imaging of the simulated helicopter signal: (a) TF representation; (b) Detection of stationary patterns; (c) Detection of tail-blades; (d) Detection of main blades region.

are simulated by signals producing lines connecting peaks of the sinusoidal FM signal with time axis. Smaller pulses that can be seen in the right hand side of Fig.9a correspond to the tail rotor flashes. These flashes correspond to periodic alignment of the main and tail rotors to maximally reflect the radar signal. Note that other effects that can be observed in a radar image, including multipath, are not considered here.

Therefore, the simplified model of the reflected UH-1D signal can be written as:

$$x(t) = x_{RIG}(t)+x_{ROT}(t)+x_{FL_M}(t)+x_{FL_T}(t),$$

where $x_{RIG}(t)$, $x_{ROT}(t)$, $x_{FL_M}(t)$ and $x_{FL_T}(t)$ represent signals caused by the rigid body, rotation of the main rotor, and the main and tail rotor flashes, respectively. Signal is considered within the interval of 400 ms, sampled with a rate of $\Delta t = 1/48000$ s. Four sinusoidal components, caused by the rigid body, are at the frequencies -10.3 kHz, -2.5 kHz, 2.3 kHz and 2.7 kHz. Two components at -0.4 kHz and 0.4 kHz correspond to the modulated time tones commonly added to the data tape [16]. Sinusoidal FM signals, corresponding to the rotation of main rotor blades, are modeled as:

$$\begin{aligned} x_{ROT}(t) = \\ = \sigma_{ROT} e^{(j2\pi A_{ROT}\sin(2\pi t/T_{ROT}))} + \\ + \sigma_{ROT} e^{(-j2\pi A_{ROT}\sin(2\pi t/T_{ROT}))}. \end{aligned} \quad (16)$$

where $T_{ROT} = 175$ ms and $A_{ROT} = 19$ kHz. The main and tail rotor flashes are modeled as a broadband pulses given as:

$$x_{FL_M}(t) = \sigma_{FL_M} \sum_k \delta(t-kT_{ROT}/2) *_t h_{FL_M}(t)$$

$$x_{FL_T}(t) = \sigma_{FL_T} \sum_k \delta(t-kT_{TAIL}/2) *_t h_{FL_T}(t), \quad (17)$$

where T_{TAIL} in our experiment is $T_{TAIL} = 35.8$ ms, while $h_{FL\_M}(t)$ and $h_{FL\_T}(t)$ are cut-off filters given in the frequency domain as:

$$H_{FL\_M}(\omega) = \begin{cases} 1 & |\omega| < 2\pi A_{ROT} \\ 0 & \text{elsewhere,} \end{cases}$$

$$H_{FL\_T}(\omega) = \begin{cases} 1 & 2\pi(7.35\,\text{kHz}) \\ & < \omega < 2\pi(15.7\,\text{kHz}) \\ 0 & \text{elsewhere.} \end{cases}$$

Signal is corrupted with moderate Gaussian noise. To compare our simulated radar image with the real one, refer to [4], [16].

The previously used form of the L-statistics can be applied for separation of the rigid body and rotating parts influence. In the case when we want to separate different effects caused by rotating parts, the modified L-statistics can be applied. The L-statistics corresponding to the smallest SPEC samples is presented in Fig.9b. As a threshold we adopted 10% of the maximal value of corresponding L-statistics. Dotted line represents the region of detected stationary patterns. For detection of the tail blades region we have considered L-statistics of 30% the highest SPEC samples for each frequency, excluding 10% the highest ones of them (Fig.9c). Again, the region is estimated based on the values that are above 10% of the maximal value of the L-statistics, but with excluded stationary components regions. Finally, the highest 10% of SPEC samples are given in Fig.9d. Based on this illustration, it is easy to determine the region of the main blades (comparing to the threshold determined as in previous cases, but not excluding any sample).

Note that the proposed approach can be used for helicopter radar signals where relatively long FM signal components appear. In the case when, in the recording, short burst components dominate, on high frequencies, without a sinusoidal FM component, wavelet transform analysis setup can be efficiently used [1].

VI. CONCLUSION

Two techniques for separation of rigid body radar image from m-D effect caused signal in ISAR imaging are proposed. The first one is based on the order statistics of the SPEC samples. In order to separate patterns caused by the rotating and rigid body parts, the SPEC is evaluated for various window sizes. The SPEC evaluated with a narrow window produces high concentration of the signal caused by rotating parts, while the SPEC evaluated for a wide window produces high concentration of the sig-

nal corresponding to the rigid body parts. The second approach is based on the RT processing of obtained radar signals. It can be useful in the case of the radar targets with a dominant m-D effect caused signals. Both proposed methods have shown satisfactory accuracy for the considered complex simulated examples, including rotating and vibrating target parts.

References

[1] T. Thayaparan, S. Abrol, and E. Riseborough: "Micro-Doppler feature extraction of experimental helicopter data using wavelet and time-frequency analysis," *RADAR 2004, Proc. of the International Conference on Radar Systems*, 2004.

[2] T. Thayaparan, S. Abrol, V. C. Chen, and E. Riseborough: "Analysis of Micro-Doppler radar signatures from experimental helicopter and human data", NATO SET-80 symposium, Oslo, Norway, Oct. 2004.

[3] J. Misiurewicz, K. Kulpa, and Z. Czekala: "Analysis of recorded helicopter echo", *IEE Radar 98, Proceedings*, pp. 449-453.

[4] V. C. Chen, F. Li, S.-S. Ho, H. Wechsler: "Analysis of micro-Doppler signatures," *IEE Proc. Radar, Sonar, Navig.*, Vol. 150, No. 4, Aug. 2003, pp. 271-276.

[5] V. C. Chen: "Micro-Doppler effect in radar: Part I: Phenomenon, physics, mathematics, and simulation study", *IEEE Trans. Aero. and El. Syst*, preprint.

[6] J. Li, H. Ling: "Application of adaptive chirplet representation for ISAR feature extraction from targets with rotating parts", *IEE Proc. Radar, Sonar, Navig.*, Vol.150, No.4, August 2003, pp.284-291.

[7] T. Thayaparan, "Micro-Doppler analysis of the rotation antenna in airborne SAR image collected by the APY-6 radar," *IRS 2005*, Berlin, Germany, Sept. 2005.

[8] W. J. Williams, E. J. Zalubas: "Invariant classification of time-frequency representations: Applications to Doppler radar target identification," in *Proc. of DSTO/DOD Workshop*, Adelaide, Austr. 1997.

[9] P. Setlur, M. Amin, T. Thayaparan: "Micro-Doppler signal estimation for vibrating and rotating targets," in *Proc. of ISSPA 2005*, Sydney, Austr. 2005, pp. 639-642.

[10] Y. Wang, H. Ling, and V. C. Chen, "ISAR motion compensation via adaptive joint time-frequency techniques," *IEEE Trans. Aerosp., Electron. Syst.*, Vol. 38, No. 2, 1998, pp. 670-677.

[11] H. A. David, H. N. Nagaraja: Order statistics, Wiley, 2003.

[12] F. Gini, G. B. Giannakis: "Hybrid FM-polynomial phase signal modeling: Parameter estimation and Cramer-Rao Bounds," *IEEE Trans. Signal Processing*, Vol. 47, No. 2, Feb. 2003, pp.363-377.

[13] I. Pitas: *Digital image processing algorithms*, Prentice Hall 1993.

[14] T. Thayaparan, G. Lampropoulos, S. K. Wong, and E. Risenborough: "Application of adaptive joint time-frequency algoritgm for focusing distorted ISAR images from simulated and measured radar data," *IEE Proc. Radar, Sonar, Navig.*, Vol. 150, No. 4, Aug. 2003, pp. 213-220.

[15] T. Sparr and B. Krane: "Micro-Doppler analysis of vibrating targets in SAR," *IEE Proc. Radar Sonar Navig.*, Vol. 150, No. 4, Aug. 2003, pp. 277-283.

[16] S. L. Marple: "Special time-frequency analysis of helicopter Doppler radar data", in *Time-Frequency Signal Analysis and Processing*, ed. B. Boashash, Elsevier 2004.